14

PHOTOABLATION OF POLYMER MATERIALS

LUKAS URECH AND THOMAS LIPPERT

Photochemistry and Photophysics of Polymer Materials, Edited by Norman S. Allen

14.1 INTRODUCTION

Laser ablation of polymers was first reported by Srinivasan and Mayne-Banton [1] and Kawamura et al. [2] in 1982. Since then, numerous reviews on laser ablation of a large variety of polymers and the different proposed ablation mechanisms have been published [3–11]. There is still an ongoing discussion about the ablation mechanisms, for example, whether it is dominated by photothermal or photochemical processes.

Since its discovery, laser polymer processing has become an important field of applied and fundamental research. The research can be separated into two fields, the investigation of the ablation mechanism and its modeling and the application of laser ablation to produce novel materials. Laser ablation is used as an analytical tool in matrix-assisted laser desorption/ionization (MALDI) [12,13] and laser-induced breakdown spectroscopy (LIBS) [14] or as preparative tool for pulsed laser deposition (PLD) of synthetic polymers [15,16] and of inorganic films [17,18].

The industrial applications for polymers in laser ablation can be divided into two main groups: in applications where a structure is produced in the polymer and into a second group, where the ablation products are of specific interest.

Structuring of polymers today is industrially used for the production of nozzles for inkjet printers [19] and to prepare via holes in multichip modules through polyimide (PI) by IBM [20], as well as for many other applications, for example, fabrication of microoptical devices [21] and microfluidic channels [22–25].

Examples for the second group are polymers as fuel in the micro laser plasma thruster (μLPT), PLD of polymers, matrix-assisted pulsed laser evaporation (MAPLE), which is a deposition technique that can be used to deposit highly uniform thin films [26], or laser-induced forward transfer (LIFT) [27–29], which can be used to produce microstructures by transferring an irradiated area of a target film to an acceptor substrate. The polymer can be the transferred material, or just functions as driving force in the transfer.

14.1.1 Fundamental Issues of Laser Ablation

For an understanding of polymer ablation the main ablation parameters have to be explained and their definition have to be discussed in detail. Also, the most frequently proposed ablation mechanisms and models will be discussed.

14.1.1.1 Ablation Parameters The main parameters that describe polymer ablation are the ablation rate, $d(F)$, and the ablation threshold fluence, F_{th}, which is defined as the minimum fluence where the onset of ablation can be observed. A third important parameter is the effective absorption coefficient, α_{eff}, which yields information on the mechanisms that take place in the ablation process when compared to the linear absorption coefficient, α_{lin}, that is measured on thin unirradiated polymer films.

The ablation process is often described by the following equation [30,31]:

$$d(F) = \frac{1}{\alpha_{\text{eff}}} \ln\left(\frac{F}{F_{\text{th}}}\right) \tag{14.1}$$

Also, the method how the ablation parameters are acquired can have a pronounced influence on the results. The ablation rate can be defined either as the depth of the ablation crater after one pulse at a given fluence, or as the slope of a linear fit of a plot of the ablation depth versus the pulse number for a given fluence. Very different ablation rates can result from the two different measurement methods. This is especially the case for materials where ablation does not start with the first pulse, but after multiple pulses, or if the ablation crater depth after one pulse is too small to be measured. The process that occurs if ablation does not start with the first laser pulse is called *incubation*. It is related to physical or chemical modifications of the material by the first few laser pulses, which often results in an increase of the absorption at the irradiation wavelength [32,33], for example, the formation of double bonds in poly (methylmethacrylate) (PMMA). Incubation is normally observed only for polymers with low absorption coefficients at the irradiation wavelength.

The method applied to measure the depth of the ablated area or the removed mass can also have an influence on the ablation parameters. If profilometric measurements (optical interferometry, mechanical stylus [34], or atomic force microscopy [35]) are used to calculate the ablation rate, a sharp ablation threshold can be defined. This is also supported by reflectivity [36] and acoustic measurements [37]. In mass loss measurements, such as mass spectrometry or with a quartz crystal microbalance (QCM), the so-called *Arrhenius tail* [38] has been observed for certain conditions. The Arrhenius tail describes a region in the very low fluence range, where a linear increase of detected ablation products is observed, which is followed by a much faster increase, that coincides with removal rates of the profilometric measurements [39].

Even if these different approaches are taken into account, it is often the case that the ablation rate cannot be defined with a single set of parameters. Therefore, one set of parameters has to be defined for each fluence range in which different processes dominate the ablation process and thereby influence the ablation rate. In Fig. 14.1, the dependence of the ablation rate on the irradiation fluence is illustrated as a generic

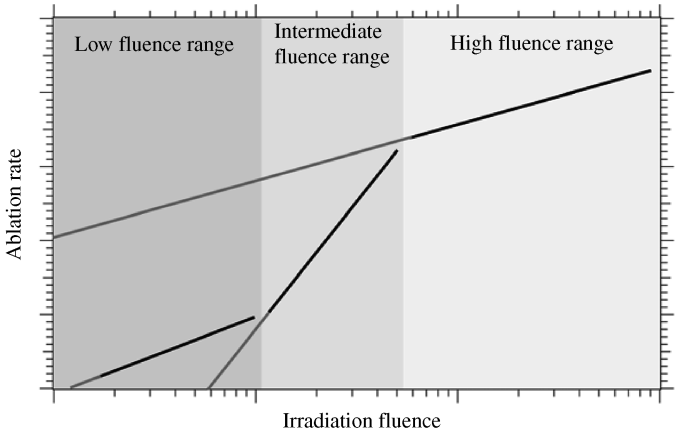

FIGURE 14.1 Schematic plot of the three fluence ranges that are typically observed for polymers. The three ranges are indicated with different shades of gray.

scheme, which is typical for most polymers. The intersection of the gray extensions of the schematic ablation rates (black lines) with the x-axis of the ablation rate versus irradiation fluence plot is the threshold fluence and varies for each fluence range. Also, a different effective absorption coefficient can be defined for each region.

Three fluence ranges are visible, which can be characterized as follows:

Low Fluence Range:

- From this fluence range, the ablation threshold fluence is normally defined.
- Incubation can be observed at these low fluences.

Intermediate Fluence Range:

- Increase of the slope of the ablation rate that is caused by a more efficient decomposition of the polymer. Energy that has been gained from an exothermic decomposition of the polymer can also increase the ablation rate.

High Fluence Range:

- The incident laser light is screened by solid, liquid, and gaseous ablation products and the laser produced plasma. This leads to similar ablation rates for many polymers [5] at high fluences.

It is therefore of great importance to consider not only the values for the different ablation parameters, but also information about the technique of analysis and for which fluence range they are valid. An interpolation to values beyond the measurement range is also not advisable, as not all three ranges have to be present for all polymers and irradiation conditions.

14.1.2 Ablation Mechanisms

Even after 25 years of research in the field of laser polymer ablation, there is still an ongoing discussion about the ablation mechanisms, for example, whether in addition to photothermal processes, photochemical reactions or even photophysical and mechanical processes are important.

It is generally accepted that for nanosecond laser pulses, the energy of the laser photons is used for electronic excitation in a first step. The following steps are still under discussion and the different models can be summarized as followed:

Photothermal: The electronic excitation is thermalized on a picosecond (ps) timescale that then results in thermal bond breaking [40–44].

Photochemical: Electronic excitation results in direct bond breaking [5,30,45–47].

Photophysical: Both thermal and nonthermal processes play a role. Two independent channels of bond breaking [48,49] or different bond breaking energies for ground-state and electronically excited-state chromophores are applied [50,51] in this model. It is most adequate for short laser pulses in the picosecond and femtosecond ranges [52].

Another way to distinguish the different models is by separating them into *surface* and *volume* models. In the volume models, the different processes that eventually result in ablation take place within the bulk of the material. In the surface models, the processes that are responsible for the material removal take place within a few monolayers below the surface. The different models can be described as follows:

Photochemical Surface Models:	Valid for long pulses and/or higher irradiation fluences [53].
Thermal Surface Models:	These models are mainly developed for metal ablation and do not consider the sharp ablation threshold, but can describe the occurrence of an *Arrhenius tail* [43,44,49,54].
Photochemical Volume Models:	These models describe a sharp ablation threshold and a logarithmic increase of the ablation crater depth with the number of laser pulses, but the *Arrhenius tail* is not accounted for [3,5,30,45,46]. A linear dependence can be described with models that consider the motion of the ablation front, but ignore the screen effects caused by the plasma plume.
Thermal Volume Models:	These models are often oversimplified by neglecting the movement of the solid–gas interface and therefore result in too high temperatures [38,42]
Volume Photothermal Model:	In this model by Arnold and Bityurin [55], a thermal surface model and a photochemical volume model have been combined. In this model, it is assumed that photothermal bond breaking takes place within the bulk polymer. When a density of broken bonds reaches a critical value, ablation begins. This model can account for sharp ablation thresholds and Arrhenius tails.

A new coarse-grained chemical reaction model (CGCRM) has been proposed by Garrison and coworkers [56,57]. In this model a kinetic Monte Carlos approache that includes a probabilistic element is used to predict when reactions occur. It is thereby possible to avoid the use of a chemically correct interaction potential. The CGCRM uses known chemical reactions along with their probabilities and exothermicities for a specific material to estimate the effect of chemical reactions on the ablation process.

A new coarse grained molecular dynamics model was developed to study the role of thermal, mechanical and chemical reactions in the onset of the ablation process of PMMA [58]. In this model, the laser energy is absorbed in different ways, i.e. pure heating and Norrish type I and II reactions. Mechanical stresses and pressure are dominant for very short pulses in the stress confinement regime and can initiate

ablation by a mechanical breakdown of the polymer in the case of pure heating. For longer pulse lengths, the ejection process is mainly thermally activated. This can be well described with thermal models based on thermally activated bond breaking processes. The presence of small molecules and gaseous products can not be accounted for by a purely thermal mechanism. A modeling of the photoablation channels requires a two-step ablation model, which incorporates the effect of photolysis of the polymer and the creation of new species, that is then followed by a thermally activated removal step.

The breathing sphere model was enhanced by Garrison and coworkers [59–62] to allow the photons to break a bond in the molecule and to describe subsequent abstraction and recombination reactions. The model was initially applied to chlorobenzene, where good correlation with experimental data was found.

The new concept that arises from these calculations is the difference in the temporal and spatial deposition of the available energy in photochemical and photothermal mechanisms. This concept provides the foundation to make specific comparisons with experiment and to explain experimental results as summarized below:

- It was found that photochemical reactions release additional energy into the irradiated sample and decrease the average cohesive energy and thereby decrease the value of the ablation threshold. The yield of emitted fragments becomes significant only above the ablation threshold.
- The presence of a shockwave with a high initial velocity, large clusters in the plume, and high velocities of particles in the plume are explained by the fast rise in energy deposition in time scales from 20 to 150 ps.
- The chemical reactions that take place above the surface after the laser pulse on longer timescales explain the higher background density in the plume with photochemical ablation than observed for photothermal ablation.
- The presence of a combination of a thermal mechanism below the ablation threshold and a volume ejection mechanism above the threshold explains why volatile products such as HCl and the matrix are only observed below threshold and all products are observed above threshold.
- The absence of heat deposited below $\sim$1.5 times the penetration depth may help to explain the cold etching process in far UV photoablation as used commercially in the corrective eye surgery, LASIK.

The different models include many material parameters and several of these parameters are obtained from fitting of experimental data and have to be adjusted to fit each polymer [9,63]. It is worth mentioning in this context that polyimide is probably the most studied polymer in laser ablation and is also the material for which most ablation models are applied, but great care has to be taken for which type of polyimide the data have been obtained. Polyimide describes a whole group of polymer that can range from soluble polymers to insoluble films and even photosensitive polymers with very different properties [10]. Even products with the same name, such as Kapton™, are not one polymer, but there are also many different types of Kapton that are defined with additional letters, for example, HN.

In general, it can be said that polymers that show a photochemical ablation behavior at the irradiation wavelength would be preferable for structuring, as the damage of the surrounding material due to a thermal processes is minimized and less carbonization is observed. A conversion of the polymer into gaseous products is also of advantage, as no or only minor amounts of ablation products are redeposited on the structured surface and additional cleaning procedures may not be necessary.

14.2 CLASSIFICATION OF POLYMERS USED FOR LASER ABLATION

Polymers can be classified in many different ways, such as their ablation behavior, the mechanisms that take place during ablation, and their suitability for selected applications.

Classification by Decomposition Behavior: The decomposition mechanism is a reasonable way to classify polymers. They can either depolymerize upon irradiation, for example, poly(methylmethacrylate), or decompose into fragments such as polyimides or polycarbonates. This method of classification is closely related to the synthesis of polymers. Polymers that are produced by radical polymerization from monomers, which contain double bonds, are likely to depolymerize into monomers, while polymers that have been formed by reactions like polycondensation will not depolymerize into monomers upon irradiation, but will be decomposed into different fragments. The second group cannot be used to produce films with the same structure or molecular weight as the original material with methods such as PLD.

Classification by the Absorber: Polymers can have intrinsic absorption at the irradiation wavelength or a dopant can be used to induce the necessary absorption. The dopant can be implemented either into the polymer matrix on a molecular level or as absorber particles in the nanometer to micrometer range. The absorbing species can also be included into the polymer backbone or side chains to increase the absorption and thereby forms a copolymer with intrinsic absorption.

By Their Availability: Many *commercially available polymers* such as poly (methylmethacrylate), poly(vinylchloride), Poly(ethylene terephthalate) (PET), and so on have been extensively studied in recent years [64], but they have several characteristics that make them unsuitable for high-quality structuring. The most prominent are low sensitivity, carbonization upon irradiation, and redeposition of ablation products on the polymer surface [65]. To improve the ablation properties for specific applications, polymers or polymer-absorber systems were designed to fit special requirements. The most important criteria for these *doped and designed polymers* for structuring are as follows:

- High absorption coefficients ($\geq$20,000 cm^{-1}) at the irradiation wavelength.
- Exothermic decomposition at well-defined positions of the polymer backbone.
- Decomposition of the polymer into gaseous products that do not contaminate the polymer surface [66,67].

14.3 LASER SOURCES

The most frequently used lasers for polymer ablation are *excimer (excited dimer)* lasers [68,69]. Their main advantages are the emission in the UV range, where most polymers reveal a high absorption, a relatively homogeneous beam profile, and the possibility to use a mask to image a small section of the laser beam on the sample. Common excimer laser wavelengths are 157 nm (F_2), 193 nm (ArF), 222 nm (KrCl), 248 nm (KrF), 308 nm (XeCl), and 351 nm (XeF) [70]. A disadvantage of excimer lasers is the limited lifetime of the gas used as laser medium that has to be exchanged quite often and thereby contributes to the high cost of the excimer laser photons. The gas has to be exchanged more often for the shorter wavelengths.

An alternative to the excimer lasers are frequency multiplied solid-state laser. The main disadvantage of these lasers is their strong coherence that makes it difficult to use a mask to cut a part of the laser beam without having diffraction patterns on the irradiated surface.

14.4 COMMERCIALLY AVAILABLE POLYMERS

14.4.1 Poly(methylmethacrylate)

A widely studied commercially available polymer is poly(methylmethacrylate) (Fig. 14.2). It is a polymer that can be completely depolymerized by heating above the ceiling temperature (T_C). It is possible only to achieve 100% monomer as product by laser irradiation with a CO_2 laser ($\lambda \approx 9.6$ or 10.6 μm) [71]. About 1% monomer can be detected in the ablation products after irradiation with 248 nm laser light, and about 18% monomer can be produced with 193 nm [71,72].

For irradiation with 308 nm, PMMA is not suitable, as it has a very low absorption coefficient at this wavelength. Structures produced with 308 nm are of poor quality [73], while for irradiation with shorter wavelengths, high-quality structures can be obtained. Ablation with 193 nm is most suitable, as no incubation is observed [74–77].

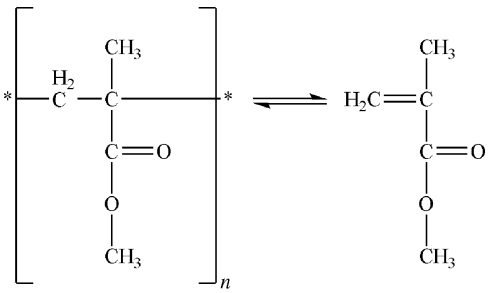

FIGURE 14.2 Chemical structure of poly(methylmethacrylate) and its monomer (right).

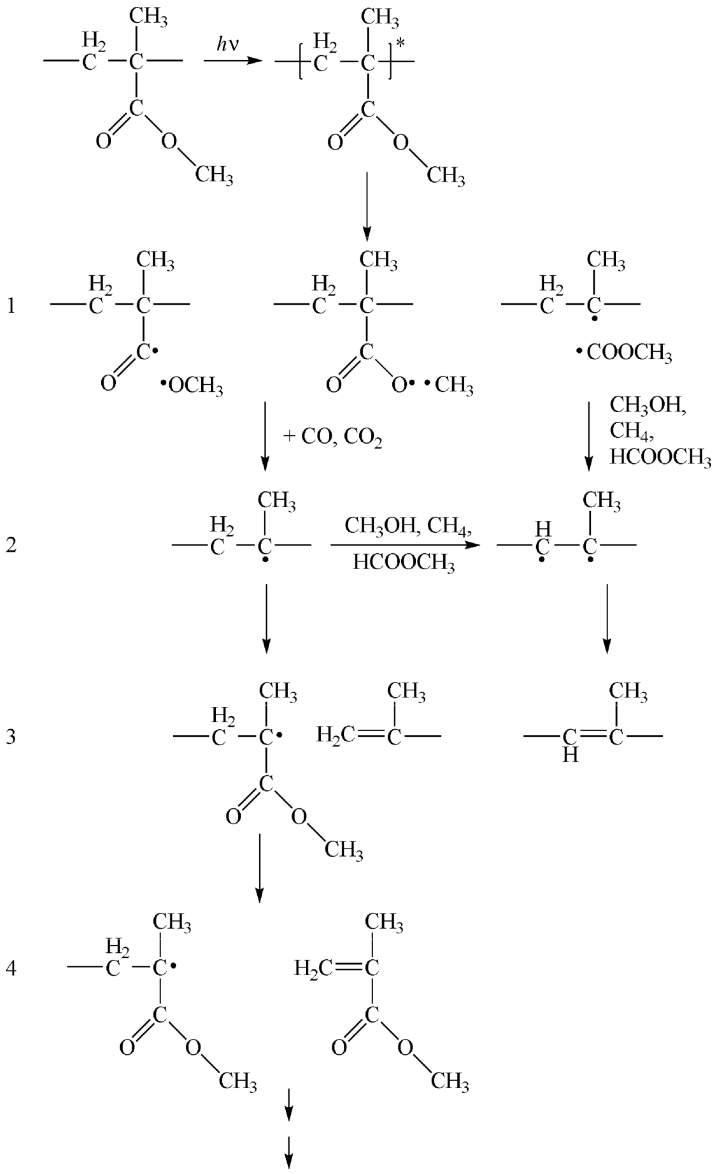

FIGURE 14.3 Proposed decomposition pathway of PMMA after irradiation with UV laser.

In Fig. 14.3, the decomposition pathway of PMMA upon irradiation with UV laser light is shown [78] as it has been defined from products detected with time-of-flight mass spectroscopy (TOF-MS). The first three steps can be associated with incubation, whereas in step 4 depolymerization takes place. Incubation, as observed for PMMA, is often present in polymers that show weak absorption at the irradiation wavelength

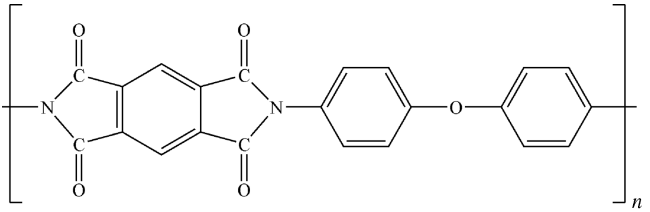

FIGURE 14.4 Chemical structure of polyimide (Kapton HN).

($\alpha_{lin} < 8000\,cm^{-1}$). It has been shown by Stuke [33] and Srinivasan [32] that during incubation a gradual increase in the absorption can be observed until ablation starts and that material is removed as vapor during incubation, even if no etching is observed.

14.4.2 Polyimide (KAPTON)

Polyimide or its most common type Kapton HN (chemical structure shown in Fig. 14.4) is the most studied polymer, as it can be ablated with all common excimer laser wavelengths and *pulse lengths* (τ). Most ablation models are based on Kapton, as its material properties are well characterized.

In nanosecond shadowgraphy measurements, a shockwave was visible for all excimer wavelengths, but the composition of the ablation plume varies with the irradiation wavelengths [79]. At 248 nm almost no solid ablation products were observed and the material removal was confined in time duration to the laser pulse. With increasing wavelengths, the amount of solid material increases. The temporal limitation of the ablation process to the laser pulse was confirmed with interferometry measurements [80]. For irradiation with 351 nm, pronounced surface swelling was observed. The swelling was then followed by the ejection of solid ablation products and a prolonged material removal. The change in the composition of the ablation plume and the duration of the ablation process has been assigned to a shift in the ablation mechanism, that is, photochemical at 248 nm to photothermal at 351 nm. No Arrhenius tail was observed with QCM measurements for 193 nm laser irradiation, which also implies a photochemical ablation process at low irradiation wavelengths. This is also in good correlation with the linear absorption coefficient of the polymer, which shows a strong decrease from $300{,}000\,cm^{-1}$ at 193 nm to about 10,000 at 351 nm (see Fig. 14.5).

Different methods, such as gas-phase FTIR [81], gas chromatography–mass spectrometry [82] and quadrupole MS [83], and emission spectroscopy [72,84], have been used to analyze the ablation products. With mass spectroscopy, fragments with masses that correspond to the following species have been detected: C_2H_2, HCN, CO, CO_2, C_4H_2, C_6H_2, C_6H_2–CN, C_6H_5–CNO, and a species at mass 153 nm that can be assigned to a cyanonaphthalene structure. With emission spectroscopy, mainly low mass species such as C_2 and CN are detected.

In industry, polyimides are widely used as dielectric in microelectronics for multichip modules [85,86] and printed circuit boards [87], as substrate for inkjet

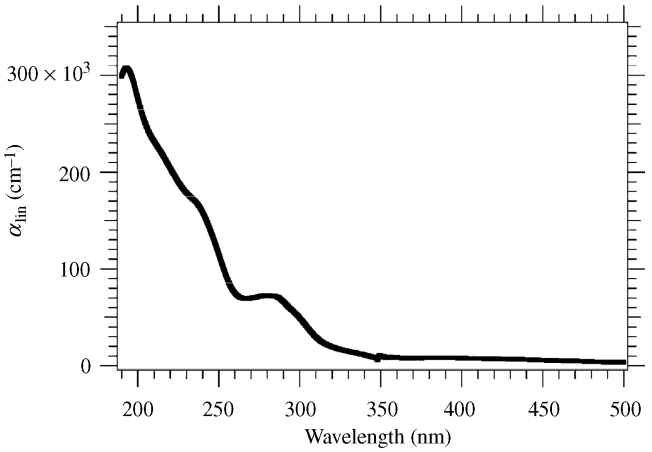

FIGURE 14.5 Linear absorption coefficient of a thin polyimide (similar to Kapton) measured from thin films.

printer nozzles [19], and as precursor for graphite materials [88]. One important feature of the polyimides is their characteristic carbonization upon laser irradiation. The carbonized material can be used to produce conduction areas on the nonconduction polymer [89,90].

14.4.3 Other Polymers

14.4.3.1 Poly(ethylene terephthalate) Poly(ethylene terephthalate) (chemical structure shown in Fig. 14.6) has been studied for most UV wavelengths (308 nm [91], 266 nm [92], 248 nm, 193 nm [93,94], and 157 nm [95]). At 157 nm, a low ablation threshold and mainly gaseous ablation products are observed, which suggests an ablation process that is dominated by photochemical reactions.

With different irradiation wavelengths, the photothermal part of the mechanism is changed and the surface crystallinity can be lowered (irradiation at 248 and 308 nm [96]) or increased with shorter wavelengths 193 nm [97].

14.4.3.2 Fluoropolymers The different fluoropolymers, poly(tetrafluoroethylene) (PTFE, Teflon, Fig. 14.7), ethylene-tetrafluoroethylene copolymers, and poly (vinylidene fluoride) (PVDF), are commercially very important polymers. The most

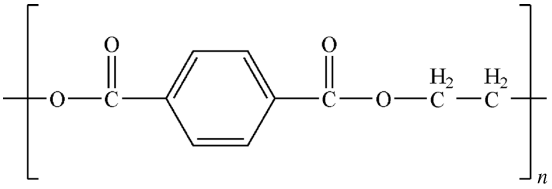

FIGURE 14.6 Chemical structure of poly(ethylene terephthalate).

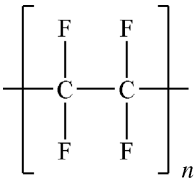

FIGURE 14.7 Chemical structure of poly(tertrafluoroethylene).

important features of PTFE are its chemical inertness, thermal stability, and hydrophobicity. It is better suited to be ablated with femtosecond laser irradiation [98], as it absorbs only weakly at wavelengths longer than 193 nm.

The ablation rate of PTFE at a constant fluence increases for irradiation between 193 and 308 nm and reaches a maximum value of 60 μm/pulse before it starts decreasing with longer wavelengths [99]. The ablation process could also be explained by applying "simple" photothermal or photochemical models.

With laser treatment in reactive atmosphere (e.g., hydrazine [100,101]) or under various liquids (e.g., $B(CH_3)_3$ [102,103]), the F–C bonds on the surface can be broken, CH_3 radicals or amino groups can be incorporated, allowing to apply a coating after laser treatment. This surface modification takes place without detectable ablation. By irradiating a PTFE foil with a F_2 laser (157 nm) in N_2 atmosphere, the surface roughness can be lowered and the transparency can be improved, without changing the film stability [104].

14.4.4 Polymer Ablation with Ultrashort Pulses

Picosecond laser pulses in the UV range do not result in better ablation behavior than nanosecond laser pulses. This is different for doped polymers. Experiments with doped PMMA (an IR-absorber, i.e., IR-165 for ablation with near-IR laser and diazomeldrum's acid (DMA) for ablation with UV lasers) with nanosecond and picosecond laser irradiation in the UV (266 nm) and near-IR (1064 nm) range have shown that, in the IR, neat features could be produced with picosecond laser irradiation, while nanosecond irradiation only results in rough surface features [105]. This corresponds well with the different behavior of the two absorbers. With IR-165 the polymer is matrix is heated by a fast vibrational relaxation and multiphonon uppumping [106]. This leads to a higher temperature jump for the picosecond irradiation, which causes ablation, while for nanosecond pulses only lower temperatures are reached.

In the UV, DMA ablation is attributed to cyclic multiphoton absorption [107] and only swelling was observed for the picosecond pulses, whereas the polymer could be ablated with nanosecond pulses.

Several studies to determine the ablation mechanisms for picosecond laser ablation were focused on spectroscopy (coherent anti-Stokes Raman scattering (CARS), absorption, and ultrafast imaging) [108–113]. It has been shown that pulses in the picosecond range produce fast temperature jumps and solid-state shockwaves that are

not observed for longer pulses. This results in pressure jumps when the film is heated faster than the hydrodynamic volume relaxation time. This pressure is then released by a rarefaction wave. The pressure produced in thin films can reach ~0.5 GPa and is generated with more or less equal amounts from shock and thermochemical decomposition. In the picosecond range, a "shock-assisted photothermal ablation" takes place.

Laser ablation with laser pulses in the femtosecond (fs) range yields unique advantages, that is, negligible heat affected zone, lower ablation threshold fluence, plasma shielding is not an issue, and the possibility to structure materials that are transparent at the irradiation wavelength.

High-quality structures can be produced in PMMA with 160 fs laser pulses at 308 nm [114], where the polymer could only be "damaged" with nanosecond pulses at the same wavelength. An ablation threshold for PMMA at 248 nm that was five times lower for 300 fs than for nanosecond pulses [115] and the structures were of better quality. Ablation of PTFE with femtosecond pulses leads to high-quality structures [98]. In the IR range, multiphoton absorption is assumed to be dominant for the ablation of PMMA and PTFE.

Near-IR solid-state lasers (e.g., Ti:sapphire) with chirped pulse amplification produce laser light with high brightness and very short pulses around 800 nm [116]. 150 fs laser pulse experiments on PI, polycarbonates (PC), PET, and PMMA have shown an increase in the single pulse ablation threshold from 1 J/cm for PI to 2.6 J/cm for PMMA. This corresponds well with the optical bandgaps of these polymers and indicates a multiphoton process. Incubation effects were observed for all polymers, but are more pronounced for PMMA, PC, and PET than for PI and PTFE, which are more stable [117–120]. Clear signs of molt redeposition of material can be observed for all polymers, except PI, which is not surprising, as it decomposes and does not melt.

14.5 DOPED POLYMERS

14.5.1 Motivation

One approach to improve the ablation behavior of commercially available polymers is to increase the absorption at the irradiation wavelength by adding an additional absorber. The ablation of doped polymers was reviewed in 1997 by Lippert et al. [121] and the polymers and the ablation mechanism were classified according to the absorption properties of the absorber-polymer system. The properties changed from systems, where only the dopant is absorbed, to systems, where absorption occurs only in the polymer. It was suggested that ablation results from a mixture of processes that originate from the polymer and the dopant. The properties of the dopant result in processes that can dominate the ablation mechanisms.

An important factor is whether the dopant is decomposing or not. A photolabile dopant that decomposes into gaseous products leads to pronounced surface swelling at low irradiation fluences, while this behavior is much less pronounced for

"photostable" dopants. Thermoelastic stress can also be induced in the polymer below the ablation threshold fluence by localized heating and thermal expansion of the polymer. This stress is then released in acoustic waves and thermal conduction into the surrounding material. The resulting transient and quasi-static thermoelastic stresses can lead to material damage and even material ejection. At high fluences, very high ablation rates [122] can be achieved, but with the drawback of pronounced surface melting. In the case of photostable dopants, less surface swelling, lower ablation rates and structures with higher quality are observed.

For all doped systems, it has to be considered that the amount of dopant is limited (typically $\leq$10 wt%) and that polymer properties such as T_g may change (to lower values).

14.5.2 Doped PMMA to Investigate the Ablation Mechanism

A higher ablation threshold fluence was found for PMMA doped with photosensitive organic compounds (iodonaphthalene and iodophenanthrene) with a higher molecular weight for irradiation with 248 nm laser light. This can be explained by the larger number of bonds that have to be broken and by the higher pressure produced by gaseous ablation products that is necessary to remove the longer fragments [123]. Also, higher surface temperatures were determined for PMMA with higher molecular weight for irradiation with 248 and 193 nm. These results can be described by a bulk photothermal model, in which a critical concentration of monomer and oligomer has to be reached before ablation occurs. This critical concentration is reached at higher temperatures for PMMA with higher molecular weight [124]. The viscosity of the polymer with different M_w in the irradiated area differs less than expected from the literature values. A strong dependence of the polymer viscosity on the molecular weight has been suggested, but the measured data reveal similar values all molecular weights. This can be explained by the higher temperatures that were observed for the higher molecular weights.

14.5.3 Doped PMMA for Structuring

Different dopants were added to PMMA to investigate the ablation mechanism during UV irradiation. The dopants that were used ranged from polyaromatic compounds to compounds that contained photochemically active groups [121].

Groups of dopants that were tested contain the triazene group (–N=N–N), as they are photochemically well studied [125–127] and also release a large amount of nitrogen when they are photochemically decomposed. Pronounced swelling has been observed by SEM analysis of the ablation craters at low irradiation fluence (Fig. 14.8, top), which is caused by gaseous products produced by the decomposition of the photolabile dopants. It has been suggested that the released nitrogen and other gaseous ablation products act as carriers for larger ablation fragments.

With increasing fluence and dopant concentration, high ablation rates of up to 80 µm can be achieved, but pronounced signs of surface melting are always visible [122] (Fig. 14.8, bottom), which is an indication for the presence of a

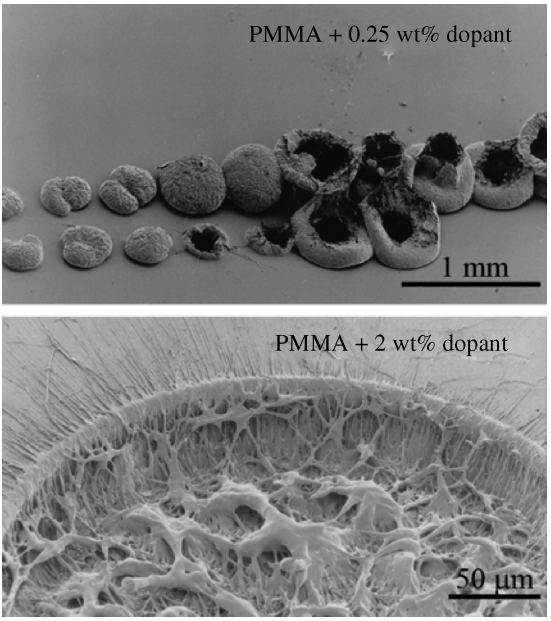

FIGURE 14.8 Irradiated PMMA with different dopant concentration after irradiation with 308 nm. In the top image, PMMA with 0.25 wt% triazene was used for ablation with one laser pulse per position. The irradiation fluence increases from left to right. Pronounced swelling and bubble formation are visible. In the bottom image, PMMA with 2 wt% is shown after two laser pulses.

photothermal mechanism. A possible reason for these pronounced thermal effects could be that the maximum amount of dopant that can be added to the polymers is $\approx$10%, which limits the achievable temperature (energy/volume).

14.5.4 Doped Polymers as Fuel for Laser Plasma Thrusters

Another quite different application utilizes dopants to induce absorption for near-IR irradiation from diode lasers. The plasma created by laser ablation of the doped polymer acts as a microthruster for small satellites. The operating principle and setup are described in detail elsewhere [128,129].

The main demand for a polymer as fuel for the plasma thruster is its exothermic decomposition. This chemically stored energy can be utilized to release higher energies in the form of thrust than the energy deposited in the polymer by the laser [130]. As absorbers for the near-IR wavelengths, carbon nanoparticles ($+$C) or IR-dyes ($+$IR) were used. As fuel polymer, glycidyl azide polymer (GAP) was studied (Fig. 14.9). GAP was originally developed as binder for solid propellant rockets [131,132], but it meets the demands for the LPT, such as easy handling, exothermic decomposition (decomposition enthalpy of -2050 J/g), and a well-defined decomposition temperature (249°C).

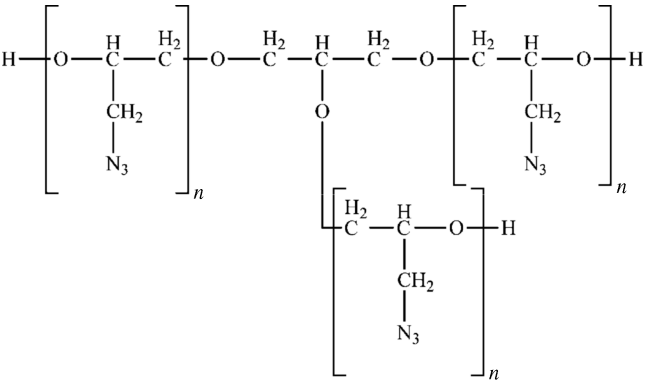

FIGURE 14.9 Chemical structure of GAP polyol.

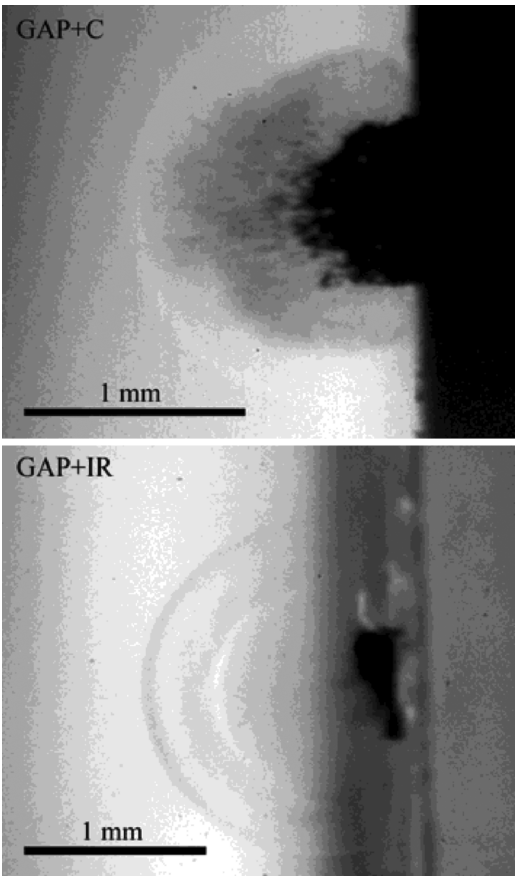

FIGURE 14.10 Shadowgraphy images of carbon (left) and IR-dye (right) doped GAP. The image was taken 1 μs after the laser pulse.

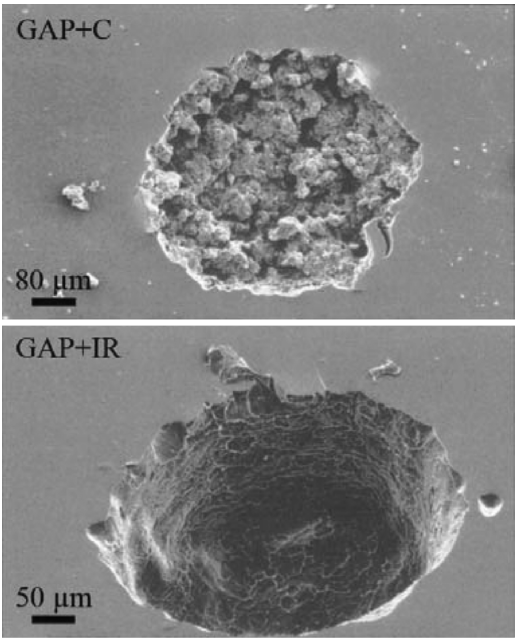

FIGURE 14.11 SEM images of the ablation spots of GAP + C (top) and GAP + IR (bottom).

The different dopants for GAP had only a small influence on the ablation properties, such as ablation rate and threshold fluence [133]. The most pronounced differences are observed in the ejected fragments detected in the shadowgraphy measurements and the ablation crater appearance. In the nanosecond-shadowgraphy image (Fig. 14.10), large fragments of solid and liquid ablation products are observed for GAP + C. In the ablation plume of GAP + IR, it seems that the ablated material is transformed completely into gaseous products. This is a desired effect, as more energy is gained by decomposing the polymer completely.

An SEM investigation of the ablation crater confirmed these results by showing an ablation crater with steep, smooth walls for GAP + IR, whereas the crater of GAP + C is quite rough, with deep holes and a very uneven bottom (Fig. 14.11).

14.6 DESIGNED POLYMERS

14.6.1 Triazene Polymers

New polymers have been developed to further improve the quality of the ablation process. One approach was to incorporate the triazene unit into the polymer backbone. A unique feature of these triazene polymers (TP, chemical structure shown in Fig. 14.12) is the possibility to adjust the absorption maximum by varying the "X"-component in Fig. 14.12 [134]. The absorption maximum of such triazene

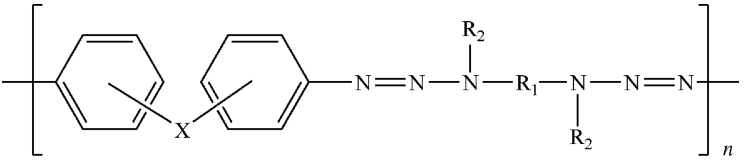

FIGURE 14.12 Chemical structure of the triazene polymers.

polymers can be tuned from 290 to 360 nm and maximum linear absorption coefficients of up to 200,000 cm^{-1} at 308 nm can be reached.

In the absorption spectra for TP1 ($X = O$, $R_1 = (CH_2)_6$, $R_2 = CH_3$) as shown in Fig. 14.13, two distinct absorption maxima can be distinguished. The R_1 and R_2 substitutes change the properties such as T_g, film forming, and chromophore density. One maximum around 200 nm, which can be assigned to the aromatic system, and the other maximum around 330 nm that corresponds to the triazene unit [135]. These two well-separated absorption regions allow an excitation of different chromophores with different irradiation wavelengths such as 193, 248, and 308 nm and thereby to study their influence on the ablation behavior.

Higher ablation rates were measured for irradiation wavelengths that excite the triazene system (266, 308, and 351 nm) compared to the ablation rates for shorter wavelengths (248 and 193 nm) [6]. Also, a clear and well-defined ablation threshold fluence of 25 mJ/cm^2 (± 5 mJ/cm^2) is observed for TP1 at an irradiation wavelength of 308 nm, while for irradiation with 248 nm a much broader range 16–28 mJ/cm^2 has been measured. For irradiation at 248 nm, carbonization of the polymer was detected upon irradiation, whereas the surface of the polymer remained unchanged after several laser pulses for irradiation with 308 nm [136]. This is also an indication for the different ablation mechanisms in the two absorption regions.

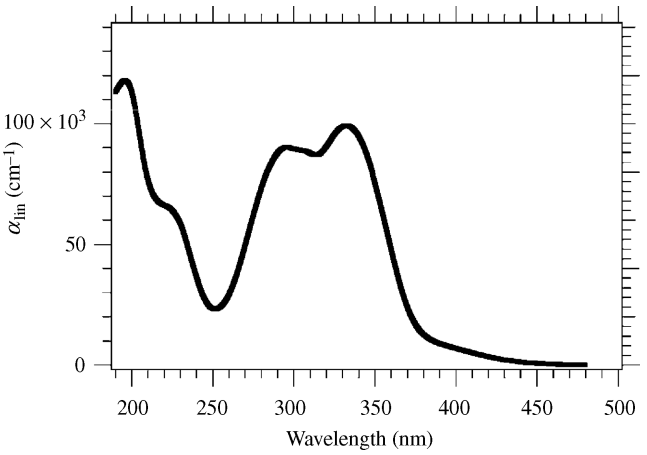

FIGURE 14.13 Linear absorption coefficient of TP1.

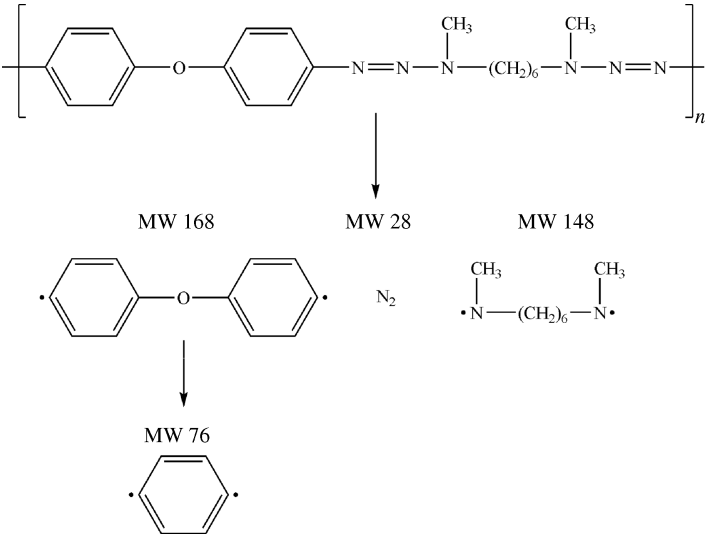

FIGURE 14.14 Decomposition pathway for TP1 measured by TOF-MS after irradiation with 308 nm.

The triazene polymers are also well suited as probes for the ablation mechanism. Mass spectrometry was used to study the ablation products and to determine the different ablation mechanisms at the different irradiation wavelengths [67,137,138]. All decomposition products were identified with time-resolved mass spectrometry for 248 and 308 nm irradiation. The proposed decomposition pathway for 308 nm irradiation is shown in Fig. 14.14, but similar products were observed also for a thermal decomposition [126]. A clearer indication for the presence of a photochemical mechanism for 308 nm irradiation was given by TOF-MS. Three different species of nitrogen were detected in the ablation plume: a very fast ground state neutral with up to 6 eV of kinetic energy, a slower ground state species with a broad energy distribution that is most probably a thermal product, and a metastable (excited) neutral N_2 species that can only be created by an electronic excitation [139].

The triazene polymers were also tested with mass spectrometry after 157 nm. These experiments showed a higher fragmentation of the polymer than for 308 or 248 nm, and even a complete fragmentation of the aromatic groups was observed [140].

The photochemical activity of the triazene group was also confirmed by irradiation at low fluences with excimer lamps, where one photon photochemistry is expected [137]. A decomposition of the triazene chromophore was observed below the ablation threshold fluence for irradiation at 308 and 222 nm. At 222 nm, an additional decomposition of the aromatic chromophores has been detected [141]. This suggests that the decomposition of the aromatic part is related to the carbonization. This selective decomposition of the triazene group by the less energetic wavelength (308 nm) clearly indicates that the triazene is the most sensitive unit in the triazene

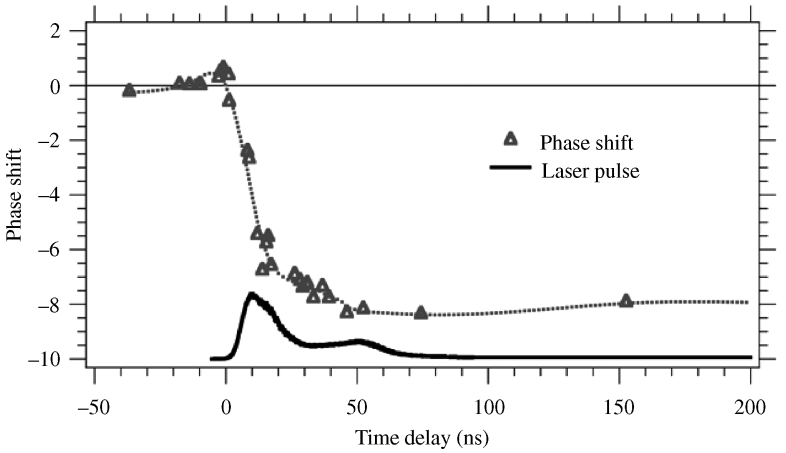

FIGURE 14.15 Interference measurement for TP1 during irradiation with 308 nm. The black curve represents the laser pulse, while the gray line corresponds to the phase shift, which is related to the ablation depth.

polymer and that a photochemical process is most probably also present during ablation.

Another method, which can be used to determine the ablation mechanism, is nanosecond interferometry. The ablation process could take place on a longer timescale (depending on the temperature) for a photothermal process than for a photochemical reaction. First, swelling is observed that is followed by etching [142,143], for example, discussed for a polyimide at 351 nm irradiation. This etching takes place on a microsecond timescale, which is much longer than the 30 ns excimer laser pulse. For the triazene polymer on the other hand, the etching starts and stops with the ablation laser pulse [141,144] (Fig. 14.15), which is again a clear indication for a photochemical process.

Irradiation experiments in the near-IR range at 800 nm with pulses in the pico- and femtosecond range were also performed. For femtosecond pulses, a lower ablation threshold fluence was found than for picosecond pulses, which indicates the presence of a thermal mechanism [145]. Also, no complete removal of a thin triazene polymer film from a glass substrate was possible with 100 fs pulses. These short pulses in the near-IR do not yield better results and are therefore no alternative to UV ablation [146].

The influence of the location of the predetermined "decomposition" site in the polymer has been tested by incorporating the triazene unit into the side chains. The obtained ablation structures were less defined, and stronger thermal effects were observed [147]. Investigation of the polymer "between" the individual triazene units suggests that a higher triazene density results in better ablation properties [7].

In Fig. 14.16, the ablation threshold fluences are plotted versus the polymer weight per triazene unit for TP1, two polyurethane polymers with the triazene unit in the polymer backbone (PUH-T1, PUH-T2 [148]), two polyacrylates with the

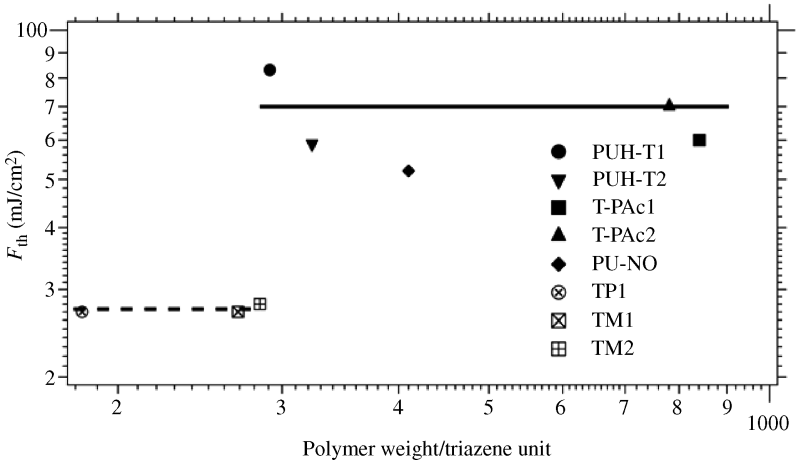

FIGURE 14.16 The ablation threshold fluence versus polymer weight per triazene unit is shown for various triazene polymers. The two lines in the plot are shown as guidelines.

triazene unit in the polymer side chain (T-PAc1, T-PAc2 [147]), two different triazene polymers with malonyl esther groups in the side chains (TM1 and TM2) [7], and a polyurethane polymer with the triazene unit in the side chain (PU-NO) [149]. A sudden increase in the ablation threshold fluence can be observed at about 285 amu/triazene group from ~25 to ~70 mJ/cm^2. Polymers above this jump have a higher ablation threshold fluence, as more bonds have to be broken to remove the larger remaining polymer fragments. Below or above this step, the ablation threshold fluence remains more or less constant, independent of the polymer weight per triazene unit. Why this sharp step is observed is not yet clear and must be studied in more detail.

14.6.2 Other Polymers Designed for Laser Ablation

Other designed polymers, such as *diazosulfidepolymer*, *pentazadienepolymer*, *diazophosphonatepolymer*, and *diazocopolyester*, have also been designed for ablation at 308 nm. All these polymers contain a photolabile chromophore based on diazo groups (–N=N–X) in the polymer main chain [150].

With all polymers, high-quality structures could be obtained, but not all polymers were stable enough to be analyzed by methods such as scanning electron microscopy. The diazosulfidepolymer could only be examined by optical microscopy, and also the pentazadienopolymer partially decomposed during sputtering prior to SEM analysis. The best results were obtained for diazocopolyester, where no incubation was observed for irradiation with 308 nm. By decreasing the triazene content below 35%, it became impossible to produce well-defined structures. The polymer started to form bubbles below the surface that were caused by a thermal decomposition of the ester into CO/CO_2 at a triazene contents above 90%.

14.7 COMPARISON OF DESIGNED AND COMMERCIALLY AVAILABLE POLYMERS

Compared to commercially available polymers such as polyimides or other designed polymers, for example, polyesters, the triazene polymers showed the highest ablation rates and the lowest ablation threshold fluence for selected wavelengths. The structure produced in TP (Fig. 14.17, top) with 308 nm irradiation are much sharper than those in Kapton (Fig. 14.17, bottom) and also no polymer debris is redeposited in and around the ablated structure in the case of the triazene polymer [141]. Kapton was chosen as commercially available reference because it has a similar α_{lin} at 308 nm. The absence of redeposited material for TP corresponds well with nanosecond-shadowgraphy measurements, where it was shown that no solid products are produced for 308 nm irradiation of TP [144].

All data obtained for TP strongly suggest that photochemical reactions play an important role during UV laser ablation, but also that photothermal processes are important. This is confirmed by the presence of the thermal N_2 products in the TOF curves. Photothermal processes will also always be present if the polymer decomposes exothermically during a photochemical decomposition and if the quantum yields of the photochemical reaction is not equal to one (which is most of time the case). The ablation of polymers will therefore always be a photophysical process (a mixture of photochemical and photothermal processes), where the ratio between the two mechanisms is a function of the irradiation wavelength and the polymer. In addition, photomechanical processes, such as pressure produced by trapped gaseous ablation products or shock and acoustic waves in the polymer, take place and can lead to a damage of the polymer and are most important for picosecond pulses.

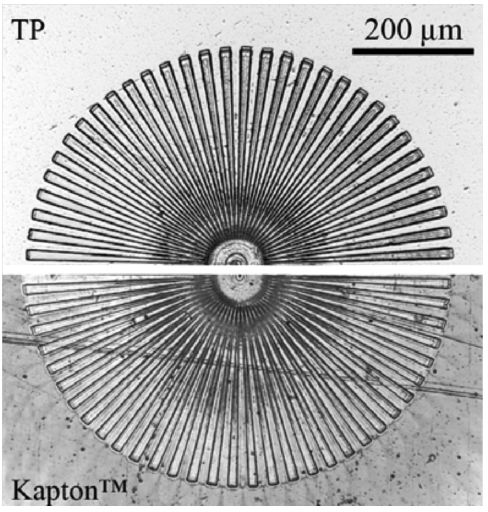

FIGURE 14.17 SEM of Siemens stars in TP (top) and Kapton (bottom), both produced with five laser pulses at 308 nm.

A more pronounced photochemical part is preferable for material structuring, as it leads to a more uniform decomposition of the polymer and results in less debris. In additional, large quantities of gaseous products are produced and less material is redeposited in and around the ablated area. The designed polymers such as the TP show a clear advantage over commercially available polymers.

REFERENCES

1. R. Srinivasan and V. Mayne-Banton *Appl. Phys. Lett.* **1982**, *41*, 576–578.
2. Y. Kawamura, K. Toyoda, and S. Namba, *Appl. Phys. Lett.* **1982**, *40*, 374–375.
3. R. Srinivasan and B. Braren *Chem. Rev.* **1989**, *89*, 1303–1316.
4. D. Bäuerle, *Laser Processing and Chemistry*, Springer Verlag, Berlin, 2000.
5. S. Lazare and V. Granier *Laser Chem.* **1989**, *10*, 25–40.
6. T. Lippert and J.T. Dickinson *Chem. Rev.* **2003**, *103*, 453–485.
7. T. Lippert, Laser application of polymers, *Polymers and Light*, Springer, Berlin, **2004**, pp. 51–246.
8. P.E. Dyer, Laser ablation of polymers in: I.W. Boyd and R.B. Jackman (Eds.), *Photochemical Processing of Electronic Materials*, Academic Press Limited, London, **1992**, pp. 360–385.
9. N. Bityurin, B.S. Luk'yanchuk, M.H. Hong, and T.C. Chong, *Chem. Rev.* **2003**, *103*, 519–552.
10. T. Lippert, *Plasma Processes Polym.* **2005**, *2*, 525–546.
11. N. Bityurin, *Annu. Rep. Prog. Chem. C,* **2005**, *101*, 216–247.
12. M. Karas, D. Bachmann, and F. Hillenkamp, *Anal. Chem.* **1985**, *57*, 2935–2939.
13. R. Zenobi and R. Knochenmuss *Mass Spectrom. Rev.* **1998**, *17*, 337–366.
14. L.J. Radziemski and D.A. Cremers (Eds.), *Laser-Induced Plasmas and Applications*, Marcel Dekker, New York, 1989.
15. G.B. Blanchet, *Chemtech* **1996**, *26*, 31–35.
16. W.B. Jiang, M.G. Norton, L. Tsung, and J.T. Dickinson, *J. Mater. Res.* **1995**, *10*, 1038–1043.
17. D.B. Chrisey and G.K. Hubler *Pulsed Laser Deposition of Thin Films*, John Wiley & Sons, New York, 1994.
18. R.W. Eason (Ed.), *Pulsed Laser Deposition of Thin Films: Applications-Led Growth of Functional Materials*, John Wiley & Son, Inc., New York, 2007.
19. H. Aoki, U.S. Patent 5736999, 1998.
20. R.S. Patel and T.A. Wassick *Proc. SPIE Int. Soc. Opt. Eng.* **2991**, *1997*, 217.
21. G. Kopitkovas, L. Urech, and T. Lippert, Fabrication of micro-optics in polymers and in UV transparent materials, in: E. Millon, J. Perriere, and E. Forgarassy (Eds.), *Recent Advances in Laser Processing of Materials*, Elsevier, Kidlington, 2006.
22. H. Klank, J.P. Kutter, and O. Geschke, *Lab Chip* **2002**, *2*, 242–246.
23. D. Snakenborg, H. Klank, and J.P. Kutter, *J. Micromech. Microeng.* **2004**, *14*, 182–189.
24. D. Gomez, F. Tekniker, I. Goenaga, I. Lizuain, and M. Ozaita, *Opt. Eng.*, **2005**, *44*.

25. D.F. Farson, H.W. Choi, C.M. Lu, and L.J. Lee, *J. Laser Appl.* **2006**, *18*, 210–215.
26. A. Pique, P. Wu, B.R. Ringeisen, D.M. Bubb, J.S. Melinger, R.A. McGill, and D.B. Chrisey, *Appl. Surf. Sci.* **2002**, *186*, 408–415.
27. T. Mito, T. Tsujita, H. Masuhara, N. Hayashi, and K. Suzuki, *Jpn. J. Appl. Phys. 2, Lett.* **2001**, *40*, L805–L806.
28. G.B. Blanchet, *Macromolecules* **1995**, *28*, 4603–4607.
29. E. Millon, J. Perriere, and E. Fogarassy (Eds.), *Recent Advances in Laser Processing of Materials*, Elsevier, Kidlington, 2006.
30. J.E. Andrew, P.E. Dyer, D. Forster, and P.H. Key, *Appl. Phys. Lett.* **1983**, *43*, 717–719.
31. R. Srinivasan and B. Braren *J. Polym. Sci. Pol. Chem.* **1984**, *22*, 2601–2609.
32. R. Srinivasan, B. Braren, and K.G. Casey, *J. Appl. Phys.* **1990**, *68*, 1842–1847.
33. S. Küper and M. Stuke *Appl. Phys. A: Mater. Sci. Process.* **1989**, *49*, 211–215.
34. S.V. Babu, G.C. Dcouto, and F.D. Egitto, *J. Appl. Phys.* **1992**, *72*, 692–698.
35. M. Himmelbauer, E. Arenholz, and D. Bauerle, *Appl. Phys. A: Mater. Sci. Process.* **1996**, *63*, 87–90.
36. G. Paraskevopoulos, D.L. Singleton, R.S. Irwin, and R.S. Taylor, *J. Appl. Phys.* **1991**, *70*, 1938–1946.
37. R.S. Taylor, D.L. Singleton, and G. Paraskevopoulos, *Appl. Phys. Lett.* **1987**, *50*, 1779–1781.
38. S. Küper, J. Brannon, and K. Brannon, *Appl. Phys. A: Mater. Sci. Process.* **1993**, *56*, 43–50.
39. T. Dumont, R. Bischofberger, T. Lippert, and A. Wokaun, *Appl. Surf. Sci.* **2005**, *247*, 115–122.
40. S.R. Cain, *J. Phys. Chem.* **1993**, *97*, 7572–7577.
41. S.R. Cain, F.C. Burns, and C.E. Otis, *J. Appl. Phys.* **1992**, *71*, 4107–4117.
42. G.C. D'Couto and S.V. Babu *J. Appl. Phys.* **1994**, *76*, 3052–3058.
43. B. Lukyanchuk, N. Bityurin, M. Himmelbauer, and N. Arnold, *Nucl. Instrum. Methods Phys. Res. B* **1997**, *122*, 347–355.
44. N. Arnold, B. Luk'yanchuk, and N. Bityurin, *Appl. Surf. Sci.* **1998**, *129*, 184–192.
45. T.F. Deutsch and M.W. Geis *J. Appl. Phys.* **1983**, *54*, 7201–7204.
46. E. Sutcliffe and R. Srinivasan *J. Appl. Phys.* **1986**, *60*, 3315–3322.
47. G.D. Mahan, H.S. Cole, Y.S. Liu, and H.R. Philipp, *Appl. Phys. Lett.* **1988**, *53*, 2377–2379.
48. V. Srinivasan, M.A. Smrtic, and S.V. Babu, *J. Appl. Phys.* **1986**, *59*, 3861–3867.
49. H. Schmidt, J. Ihlemann, B. Wolff-Rottke, K. Luther, and J. Troe, *J. Appl. Phys.* **1998**, *83*, 5458–5468.
50. B. Lukyanchuk, N. Bityurin, S. Anisimov, N. Arnold, and D. Bauerle, *Appl. Phys. A: Mater. Sci. Process.* **1996**, *62*, 397–401.
51. B. Lukyanchuk, N. Bityurin, S. Anisimov, and D. Bauerle, *Appl. Phys. A: Mater. Sci. Process.* **1993**, *57*, 367–374.
52. N. Bityurin, A. Malyshev, B. Luk'yanchuk, S. Anisimov, and D. Bäuerle, *Proc. SPIE.* **2802**, *1996*, 103.
53. N. Bityurin, *Appl. Surf. Sci.* **1999**, *139*, 354–358.

54. G.V. Treyz, R. Scarmozzino, and R.M. Osgood, *Appl. Phys. Lett.* **1989**, *55*, 346–348.
55. N. Arnold and N. Bityurin *Appl. Phys. A: Mater. Sci. Process.* **1999**, *68*, 615–625.
56. Y.G. Yingling and B.J. Garrison *J. Phys. Chem. B* **2005**, *109*, 16482–16489.
57. Y.G. Yingling and B.J. Garrison *J. Phys. Chem. B* **2004**, *108*, 1815–1821.
58. M. Prasad, P. Conforti, and B.J. Garrison, *J. Appl. Phys.* **2008**, *103*, 103114.
59. Y.G. Yingling, L.V. Zhigilei, and B.J. Garrison, *J. Photochem. Photobiol. A* **2001**, *145*, 173–181.
60. L.V. Zhigilei, E. Leveugle, B.J. Garrison, Y.G. Yingling, and M.I. Zeifman, *Chem. Rev.* **2003**, *103*, 321–347.
61. Y.G. Yingling and B.J. Garrison *Chem. Phys. Lett.* **2002**, *364*, 237–243.
62. Y.G. Yingling and B.J. Garrison *Nucl. Instrum. Methods Phys. Res. B*, **2003**, *202*, 188–194.
63. N. Bityurin and A. Malyshev *J. Appl. Phys.* **2002**, *92*, 605–613.
64. K. Suzuki, M. Matsuda, T. Ogino, N. Hayashi, T. Terabayashi, and K. Amemiya, *Proc. SPIE.* **2999**, *1997*, 98.
65. T. Lippert, M. Hauer, C.R. Phipps, and A. Wokaun, *Appl. Phys. A: Mater. Sci. Process.* **2003**, *77*, 259–264.
66. L.S. Bennett, T. Lippert, H. Furutani, H. Fukumura, and H. Masuhara, *Appl. Phys. A: Mater. Sci. Process.* **1996**, *63*, 327–332.
67. T. Lippert, S.C. Langford, A. Wokaun, G. Savas, and J.T. Dickinson, *J. Appl. Phys.* **1999**, *86*, 7116–7122.
68. O. Svelto, *Principles of Lasers*, Plenum Press, New York, **1998**.
69. F.W. Kneubühl and M.W. Sigrist *Laser*, Teubner Studienbücher Physik, Stuttgart, **1999**.
70. D. Basting (Ed.), *Excimer Laser Technology: Laser Sources, Optics, Systems and Applications*, Lambda Physics, Göttingen, **2001**.
71. R. Srinivasan, *J. Appl. Phys.* **1993**, *73*, 2743–2750.
72. R. Srinivasan, B. Braren, D.E. Seeger, and R.W. Dreyfus, *Macromolecules* **1986**, *19*, 916–921.
73. T. Efthimiopoulos, C. Kiagias, G. Heliotis, and E. Helidonis, *Can. J. Phys.* **2000**, *78*, 509–519.
74. A. Costela, J.M. Figuera, F. Florido, I. Garciamoreno, E.P. Collar, and R. Sastre, *Appl. Phys. A: Mater. Sci. Process.* **1995**, *60*, 261–270.
75. N. Bityurin, S. Muraviov, A. Alexandrov, and A. Malyshev, *Appl. Surf. Sci.* **1997**, *110*, 270–274.
76. H. Schmidt, J. Ihlemann, K. Luther, and J. Troe, *Appl. Surf. Sci.* **1999**, *139*, 102–106.
77. R.J. Lade, I.W. Morley, P.W. May, K.N. Rosser, and M.N.R. Ashfold, *Diamond Relat. Mater.* **1999**, *8*, 1654–1658.
78. T. Lippert, R.L. Webb, S.C. Langford, and J.T. Dickinson, *J. Appl. Phys.* **1999**, *85*, 1838–1847.
79. R. Srinivasan, *Appl. Phys. A: Mater. Sci. Process.* **1993**, *56*, 417–423.
80. T. Lippert, C. David, M. Hauer, T. Masubuchi, H. Masuhara, K. Nomura, O. Nuyken, C. Phipps, J. Robert, T. Tada, K. Tomita, and A. Wokaun, *Appl. Surf. Sci.* **2002**, *186*, 14–23.

81. R. Srinivasan, R.R. Hall, W.D. Loehle, W.D. Wilson, and D.C. Allbee, *J. Appl. Phys.* **1995**, *78*, 4881–4887.
82. D.L. Singleton, G. Paraskevopoulos, and R.S. Irwin, *J. Appl. Phys.* **1989**, *66*, 3324–3328.
83. S. Lazare, W.P. Guan, and D. Drilhole, *Appl. Surf. Sci.* **1996**, *96-8*, 605–610.
84. E.E. Ortelli, F. Geiger, T. Lippert, J. Wei, and A. Wokaun, *Macromolecules* **2000**, *33*, 5090–5097.
85. F. Bachman, *Chemtronics* **1989**, *4*, 149.
86. J.R. Lankard and G. Wolbold *Appl. Phys. A: Mater. Sci. Process.* **1992**, *54*, 355–359.
87. A. Beuhler, A. Tungare, and J. Savic, *Circuit World* **1998**, *24*, 36.
88. M. Inagaki, T. Takichi, Y. Hishiyama, and A. Obslei, *Chemistry and Physics of Carbon*, Marcel Dekker, New York, 1999.
89. Z. Ball and R. Sauerbrey *Appl. Phys. Lett.* **1994**, *65*, 391–393.
90. G.H. Wynn and A.W. Fountain *J. Electrochem. Soc.* **1997**, *144*, 3769–3772.
91. S. Klose, E. Arenholz, J. Heitz, and D. Bauerle, *Appl. Phys. A: Mater. Sci. Process.* **1999**, *69*, S487–S490.
92. N. Mansour and K.J. Ghaleh *Appl. Phys. A: Mater. Sci. Process.* **2002**, *74*, 63–67.
93. F. Wagner and P. Hoffmann *Appl. Surf. Sci.* **2000**, *154*, 627–632.
94. F. Wagner and P. Hoffmann *Appl. Phys. A: Mater. Sci. Process.* **1999**, *69*, S841–S844.
95. P.E. Dyer, G.A. Oldershaw, and D. Schudel, *J. Phys. D-Appl. Phys.* **1993**, *26*, 323–325.
96. T. Lippert, F. Zimmermann, and A. Wokaun, *Appl. Spectrosc.* **1993**, *47*, 1931–1942.
97. J.S. Rossier, P. Bercier, A. Schwarz, S. Loridant, and H.H. Girault, *Langmuir* **1999**, *15*, 5173–5178.
98. S. Küper and M. Stuke *Appl. Phys. Lett.* **1989**, *54*, 4–6.
99. N. Huber, J. Heitz, and D. Bauerle, *Eur. Phys. J.: Appl. Phys* **2004**, *25*, 33–38.
100. H. Niino, H. Okano, K. Inui, and A. Yabe, *Appl. Surf. Sci.* **1997**, *110*, 259–263.
101. H. Niino and A. Yabe *Appl. Phys. Lett.* **1993**, *63*, 3527–3529.
102. M. Okoshi, M. Murahara, and K. Toyoda, *J. Mater. Res.* **1992**, *7*, 1912–1916.
103. M. Murahara and K. Toyoda *J. Adhes. Sci. Technol.* **1995**, *9*, 1601–1609.
104. T. Gumpenberger, J. Heitz, D. Bauerle, and T.C. Rosenmayer, *Europhys. Lett.* **2005**, *70*, 831–835.
105. C. Hahn, T. Lippert, and A. Wokaun, *J. Phys. Chem. B*, **1999**, *103*, 1287–1294.
106. X.N. Wen, W.A. Tolbert, and D.D. Dlott, *Chem. Phys. Lett.* **1992**, *192*, 315–320.
107. H. Fujiwara, H. Fukumura, and H. Masuhara, *J. Phys. Chem.* **1995**, *99*, 11844–11853.
108. H. Kim, J.C. Postlewaite, T.H. Zyung, and D.D. Dlott, *Appl. Phys. Lett.* **1989**, *54*, 2274–2276.
109. T. Zyung, H. Kim, J.C. Postlewaite, and D.D. Dlott, *J. Appl. Phys.* **1989**, *65*, 4548–4563.
110. X.N. Wen, D.E. Hare, and D.D. Dlott, *Appl. Phys. Lett.* **1994**, *64*, 184–186.
111. D.E. Hare, J. Franken, D.D. Dlott, E.L. Chronister, and J.J. Flores, *Appl. Phys. Lett.* **1994**, *65*, 3051–3053.
112. D.E. Hare, J. Franken, and D.D. Dlott, *J. Appl. Phys.* **1995**, *77*, 5950–5960.
113. I.Y.S. Lee, X.N. Wen, W.A. Tolbert, D.D. Dlott, M. Doxtader, and D.R. Arnold, *J. Appl. Phys.* **1992**, *72*, 2440–2448.

114. R. Srinivasan, E. Sutcliffe, and B. Braren, *Appl. Phys. Lett.* **1987**, *51*, 1285–1287.
115. S. Küper and M. Stuke, *Appl. Phys. B: Photophys. Laser Chem.* **1987**, *44*, 199–204.
116. J.D. Bonlie, F. Patterson, D. Price, B. White, and P. Springer, *Appl. Phys. B: Lasers Opt.* **2000**, *70*, S155–S160.
117. S. Baudach, J. Bonse, and W. Kautek, *Appl. Phys. A*, **1999**, *69*, S395.
118. S. Baudach, J. Bonse, J. Kruger, and W. Kautek, *Appl. Surf. Sci.* **2000**, *154*, 555–560.
119. J. Bonse, S. Baudach, J. Krüger, and W. Kautek, *Proc. SPIE Int. Soc. Opt. Eng.* **2000**, *4065*, 161.
120. S. Baudach, J. Krüger, and W. Kautek, *Rev. Laser Engin.* **2001**, *29*, 705.
121. T. Lippert, A. Yabe, and A. Wokaun, *Adv. Mater.* **1997**, *9*, 105–119.
122. T. Lippert, A. Wokaun, J. Stebani, O. Nuyken, and J. Ihlemann, *Angew. Makromol. Chem.* **1993**, *213*, 127–155.
123. G. Bounos, A. Selimis, S. Georgiou, E. Rebollar, M. Castillejo, and N. Bityurin, *J. Appl. Phys.* **2006**. *100*.
124. G. Bounos, A. Athanassiou, D. Anglos, and S. Georgiou, *Chem. Phys. Lett.* **2006**, *418*, 317–322.
125. T. Lippert, J. Stebani, O. Nuyken, A. Stasko, and A. Wokaun, *J. Photochem. Photobiol. A*, **1994**, *78*, 139–148.
126. O. Nuyken, J. Stebani, T. Lippert, A. Wokaun, and A. Stasko, *Macromol. Chem. Phys.* **1995**, *196*, 751–761.
127. A. Stasko, V. Adamcik, T. Lippert, A. Wokaun, J. Dauth, and O. Nuyken, *Makromol. Chem. Macromol. Chem. Phys.* **1993**, *194*, 3385–3391.
128. C.R. Phipps, J.R. Luke, G.G. McDuff, and T. Lippert, *Proc. SPIE* **2002**, *4760*, 833–842.
129. T. Lippert, C. David, M. Hauer, A. Wokaun, J. Robert, O. Nuyken, and C. Phipps, *J. Photochem. Photobiol. A* **2001**, *145*, 87–92.
130. L. Urech, T. Lippert, C. Phipps, and A. Wokaun, *Appl. Surf. Sci.* **2007**, *253*, 7646.
131. J. Köhler and R. Meyer *Explosivstoffe*, Wiley-VCH, Weinheim, 1998.
132. M.B. Frankel, L.R. Grant, and J.E. Flanagan, *J. Propul. Power* **1992**, *8*, 560–563.
133. L. Urech, M. Hauer, T. Lippert, C.R. Phipps, E. Schmid, A. Wokaun, and I. Wysong, *Proc. SPIE* **2004**, *5448*, 52–64.
134. O. Nuyken, J. Stebani, T. Lippert, A. Wokaun, and A. Stasko, *Macromol. Chem. Phys.* **1995**, *196*, 739–749.
135. T. Lippert, L.S. Bennett, T. Nakamura, H. Niino, A. Ouchi, and A. Yabe, *Appl. Phys. A: Mater. Sci. Process.* **1996**, *63*, 257–265.
136. T. Lippert, T. Nakamura, H. Niino, and A. Yabe, *Appl. Surf. Sci.* **1997**, *110*, 227–231.
137. T. Lippert, C. David, J.T. Dickinson, M. Hauer, U. Kogelschatz, S.C. Langford, O. Nuyken, C. Phipps, J. Robert, and A. Wokaun, *J. Photochem. Photobiol. A,* **2001**, *145*, 145–157.
138. T. Lippert, A. Wokaun, S.C. Langford, and J.T. Dickinson, *Appl. Phys. A: Mater. Sci. Process.* **1999**, *69*, S655–S658.
139. M. Hauer, T. Dickinson, S. Langford, T. Lippert, and A. Wokaun, *Appl. Surf. Sci.* **2002**, *197*, 791–795.

140. M. Kuhnke, L. Cramer, J.T. Dickinson, T. Lippert, and A. Wokaun,TOF-MS study of photoreaktive polymers ablated by F_2 excimer laser (157 nm). *Poster at COLA*, 2003, Kreta.

141. T. Lippert, J.T. Dickinson, M. Hauer, G. Kopitkovas, S.C. Langford, H. Masuhara, O. Nuyken, J. Robert, H. Salmio, T. Tada, K. Tomita, and A. Wokaun, *Appl. Surf. Sci.* **2002**, *197*, 746–756.

142. H. Furutani, H. Fukumura, and H. Masuhara, *J. Phys. Chem.* **1996**, *100*, 6871–6875.

143. H. Furutani, H. Fukumura, H. Masuhara, S. Kambara, T. Kitaguchi, H. Tsukada, and T. Ozawa, *J. Phys. Chem. B,* **1998**, *102*, 3395–3401.

144. M. Hauer, D.J. Funk, T. Lippert, and A. Wokaun, *Appl. Surf. Sci.* **2003**, *208*, 107–112.

145. J. Bonse, S.M. Wiggins, J. Solis, and T. Lippert, *Appl. Surf. Sci.* **2005**, *247*, 440–446.

146. J. Bonse, S.M. Wiggins, J. Solis, T. Lippert, and H. Sturm, *Appl. Surf. Sci.* **2005**, *248*, 157–162.

147. E.C. Buruiana, T. Buruiana, H. Lenuta, T. Lippert, L. Urech, and A. Wokaun, *J. Polym. Sci. Pol. Chem.* **2006**, *44*, 5271–5282.

148. E.C. Buruiana, V. Melinte, T. Buruiana, B. Simonescu, T. Lippert, and L. Urech, *J. Photochem. Photobiol.* **2007**, *A186*, 270.

149. E.C. Buruiana, V. Melinte, T. Buruiana, T. Lippert, H. Yoshikawa, and H. Mashuhara, *J. Photochem. Photobiol. A,* **2005**, *171*, 261–267.

150. T. Lippert, T. Kunz, C. Hahn, and A. Wokaun, *Recent Res. Dev. Macromol. Res.* **1997**, *2*, 121.